

## A study of the effect of preres relaxation on the nanoindentation process of crystalline copper

M. MAŹDZIARZ, T. D. YOUNG, G. JURCZAK

*Department of Computational Science  
Institute of Fundamental Technological Research  
Polish Academy of Sciences  
Pawińskiego 5b  
02-106 Warsaw, Poland  
e-mails: mmazdz@ippt.gov.pl, tyoung@ippt.gov.pl, gjurcz@ippt.gov.pl*

THIS PAPER EXAMINES how preres relaxation effects the development of the mechanics of a nanoindentation simulation. In particular, the force-depth relation, indentation stress-strain curves, hardness and elastic modulus, are investigated through molecular statics simulations of a nanoindentation process, starting from initial relaxation by: (i) molecular dynamics and (ii) molecular statics. It is found that initial relaxation conditions change the quantitative response of the system, but not the qualitative response of the system. This has a significant impact on the computational time and quality of the residual mechanical behaviour of the system. Additionally, the method of determining of the elastic modulus is examined for the spherical and planar indenter; and the numerical results are compared. An overview of the relationship between the grain size and hardness of polycrystalline copper is examined and conclusions are drawn.

**Key words:** molecular statics, molecular dynamics, nanoindentation, copper.

Copyright © 2011 by IPPT PAN

### 1. Introduction

THE OBJECT OF THE PAPER is to examine the influence of the method of preparation of an atomistic model, to be subject to nanoindentation by considering two standard types of preres relaxation. After preres relaxation, the sample is taken into a nanoindentation process governed by molecular statics (MS), that drives the atomistic structure away from equilibrium (see [17]). The nanoindentation process, because of its importance as a measuring technique, is a good ground on which we can perform computational optimisation tests. Numerical simulation of the nanoindentation process helps to explain the mechanisms responsible for deformations, which are not available for direct observation and in particular, show a lack of continuity in the force-depth curves for the load-unload cycle. These phenomena are inextricably linked to the atomistic structure of the material and

manifest themselves in the form of structural dislocations. The resultant physical properties following the mechanical forces are investigated: hardness, elastic modulus, the force-indentation depth, and the indentation stress-strain curves (in the context visited in this work, see also [6, 12, 32]).

This investigation determines whether prerelaxation via molecular dynamics (MD) is necessary for a computable atomistic-scale sample, and whether an instantaneous relaxation through MS is sufficient to describe the same process. In fact, due to the limitations of MD, e.g. time scales, spatial scales, very high strain rates, the lack of conservation of energy during the simulation, the problem of artificial reflected waves, its use is often questioned. It is peculiar that MS [5, 11, 17] is used much less frequently than MD [16, 28, 33] as a prerelaxation tool, since MS does not suffer this kind of drawbacks. Furthermore, MS is often used as a method of “hard” verification for checking whether the solution obtained by MD is “correct” and as a method to simulate molecular phenomena, where MD can not be used because of its limitations. Following the conclusions of [32], it is noted that awareness of the reliability of MS/MD as a general problem is paramount to successful simulation of materials and that no holistic solution exists. It is rather the case that numerical experimentation is required for each specific case under investigation. For an exploration and comparative monologue of the features of MD and MS, differences between the two methods, and proposed areas of applicability, the Reader is referred to *The Handbook of Materials Modelling* [34].

Continuing this line of thought, while there is no doubt that MD has its own merits, one is led to the question; “Is there a need for the MD prerelaxation for *this* kind of simulation?”. To probe that question with the nanoindentation simulation in mind, two methods of prerelaxation are investigated utilising the Tight-Binding (TB) inter-atomic potential. These are:

1. MD is used to prerelax an atomic mesh prior to nanoindentation simulation with a *NVT*-type thermostat [30] i.e. constant particle number  $N$ , constant volume  $V$ , and cooling temperature, to minimise the energy of kinetic vibrations in the range, from  $T_{\text{start}} = 300$  K to  $T_{\text{end}} = 1$  K.
2. MS is used to allow the atoms to settle in their equilibrium positions as a initial step of the nanoindentation simulation. This is equivalent to starting of the nanoindentation with a not relaxed atomic mesh, and allowing the system to relax itself at the moment when nanoindentation begins.

As sketched above, the prescribed MS scheme does not require a separate model for prerelaxation, which turns out to be a significant practical advantage. To distinguish between that and the former method of prerelaxation by MD, this (MS) is to be referred to as an *instantaneous relaxation* scheme in remainder of this paper.

In many fields of computational science, a method for speed-up, while not sacrificing the accuracy of the simulation, is highly desirable. It is therefore not

without significance that the time needed for a MD prerelaxation is comparable with total time of a MS simulation of the nanoindentation process. Added to that: nanoindentation simulations are by themselves time-consuming and where a statistical approach is chosen, in which many simulations are performed with slightly varying initial conditions as their only difference; a small significant change in computational time becomes a large significant change in the simulation as a whole.

The computational speed-up obtained in the case when instantaneous relaxation was applied (2 hours compared with 12 hours in the case of prerelaxation via MD), is a notable advantage for statistically-based investigations of the nanoindentation process; but if and only if it can be demonstrated that a particular model can produce comparable results for both prerelaxed models. Thus, the prerelaxation and the instantaneous relaxation schemes are set side-by-side in comparison of the indentation force-depth curve for loading-unloading of mono- and polycrystalline structures. It is found that in this case, the MS scheme is a sufficient framework to use as a prerelaxation tool for computational mechanics, where non-equilibrium systems are to be simulated.

## 2. Numerical simulations

Four distinct copper samples are considered in this work: one monocrystal and three polycrystals. As sketched above, each sample type is prerelaxed by MD or instantaneously relaxed by MS and then indented with an indenter of radius 4 nm which, known through experience [17], is small enough to limit the influence of boundary constraints during indentation, and large enough to prevent localisation of deformations.

As a starting point for the monocrystalline sample, a primitive cell of fcc (face-centred cubic) copper is replicated 56 times in the  $xy$ -plane direction and 28 times in the  $z$ -direction, leading to a supercell size of  $202.54 \times 202.54 \times 101.27 \text{ \AA}$  with  $\sim 0.4 \times 10^6$  atoms; see Fig. 1a). Generation of polycrystalline structure was based on a Voronoi-type tessellation [13, 17, 20]. Seeds are randomly placed in a supercell of dimension equal to that of the monocrystalline sample, with a crystal lattice orientation determined by three Euler angles. A copy of the original configuration is rotated around the seed, cut-out by a truncated octahedron around the seed, and finally assembled together. Atoms which protrude beyond the supercell boundaries are dismissed. In this manner, three superlattice sites with different grain sizes 6.9, 4.4, and 3.2 nm are created; see Fig. 1b–d, respectively. Grain boundaries created in a geometrical way usually have a structure that is less dense than those observed in real materials. In order to improve the initial configuration and to move atoms at grain boundaries to their energetically favourable positions, the complete structure is prerelaxed by one of the afore-

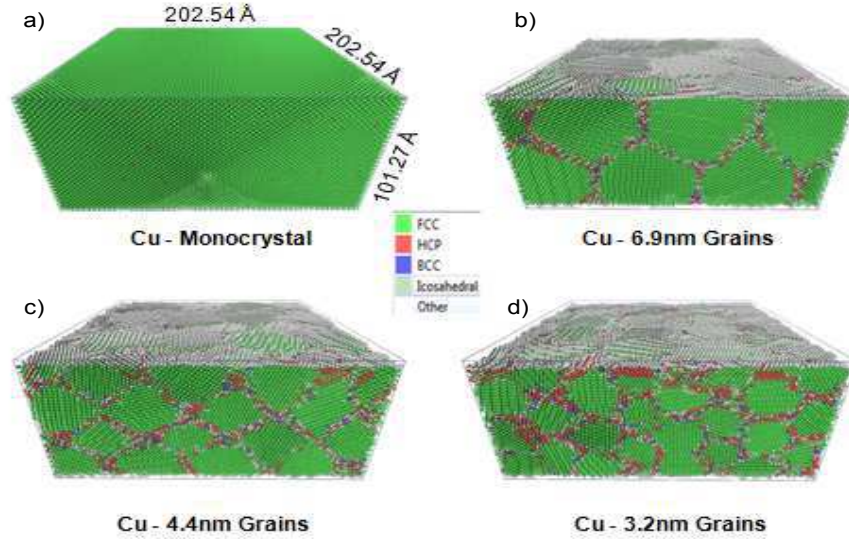


Fig. 1. Ball model illustration of the copper samples used in this work: a) monocrystal, b) 6.9 nm, c) 4.4 nm, d) 3.2 nm grain size polycrystals. Colouring of balls is given by the Ackland parameter [1, 26], Green balls denote atoms connected with the fcc phase of copper (monocrystal), red, blue, and light-blue balls denote HCP, BCC, and Icosahedral phases of copper, respectively. White balls are those with no clearly associated phase (other).

mentioned methods (cf. Section 1). For all cases (prerelaxation and indentation), periodic boundary constraints are applied to side facets, whereas the base of the sample is fixed and the upper surface is left free [30]. During the prerelaxation process, the upper surface become rough due to coalescence on grain boundaries, whereas the side walls and base remain regular; see Fig. 1b–d, respectively.

A relatively simple scheme for dealing with atomic structure in prerelaxation and nanoindentation schemes, is the Second Moment Approximation (SMA) of the TB potential [3, 17]. The so-called TB-SMA potential is parametrised for an  $N$ -atom system with interatomic separation  $r_{ij}$ , in which the total energy of the system  $E_0 = \sum_i^N E_i$  is the sum of the repulsive and attractive terms

$$(2.1) \quad E_i = \sum_j A e^{-p(\frac{r_{ij}}{r_0}-1)} - \left( \sum_j \xi^2 e^{-2q(\frac{r_{ij}}{r_0}-1)} \right)^{1/2},$$

between the  $i$ th atom and its nearest  $j$ th neighbour. The parameters for equilibrium fcc-copper crystal are:  $A = 0.0855$  eV,  $\xi = 1.224$  eV,  $p = 10.960$ ,  $q = 2.278$  [3], and  $r_0 = 2.556$  Å. A cut-off parameter for the inter-atomic potential  $r_c = 5.0$  Å was chosen and from that, the three independent elastic constants for fcc copper were calculated to be in reasonable agreement with expectation; namely,  $C_{11} = 168.76$  GPa,  $C_{12} = 120.08$  GPa, and  $C_{44} = 74.48$  GPa [22].

### 3. Nanoindentation

In nanoindentation, by experiment or simulation, the depth of penetration of a nanoindenter is measured along with the prescribed load. The resulting load-displacement response typically behaves as an elasto-plastic process at loading, followed by elastic unloading. The elastic equations of contact are then used in conjunction with the unloading data to determine the elastic modulus and hardness of the specimen [7]. The energy of each particle (atom) interacting with the spherical indenter is:

$$(3.1) \quad E(r) = -\frac{K}{3}(r - R)^3,$$

where  $K = 3.0 \text{ eV}/\text{\AA}^3$  is an energy density constant [35, 36]. The radial force  $F$  exerted by a spherical indenter, of radius  $R$  on an atom of distance  $r$  to the centre of the indenter, can be determined by the energy derivative:  $dE/dr$ . The force is repulsive and  $F(r) = 0$  for  $r > R$ . In our case, the spherical indenter impinges on the restrained sample with steps  $\Delta h = 0.5 \text{ \AA}$  to a maximum depth equal to  $20 \text{ \AA}$  and then drawn back until the force acting on indenter vanishes.

Most theories dealing with spherical nanoindentation surround the Hertz equation in the elastic region [18]. If it is assumed that at the initial stage of indentation the model behaves as an elastic material (see Fig. 2), the effective indentation modulus  $E_{\text{eff}}$  can be determined directly from the relation describing the indentation force:

$$(3.2) \quad F = \frac{4}{3}E_{\text{eff}}R^{1/2}h_e^{3/2},$$

and otherwise determined from the unloading curve, which is treated as purely elastic. For the unloading elastic curve  $h_e = h_{\text{max}} - h_r$  and, following [7, 10, 21, 25], the unloading elastic curve can then be approximated by:

$$(3.3) \quad F = \alpha(h - h_r)^m,$$

where  $\alpha$  and  $m$  are constants, and from which the contact stiffness  $S$  follows as the first derivative of the indentation force

$$(3.4) \quad S = \frac{dF}{dh} = \alpha m(h - h_r)^{m-1}.$$

The approximation of Eq. (3.3) to the unloading curve gives for monocrystalline sample  $\alpha = 628.36$  and  $m = 2.2$ , see Fig. 2c). By  $S_{\text{max}}$  we denote contact stiffness for the maximum applied force  $F_{\text{max}}$  from which the contact depth can be computed by:

$$(3.5) \quad h_c = h_{\text{max}} - \frac{h_e}{2} = h_{\text{max}} - \frac{3 F_{\text{max}}}{4 S_{\text{max}}}.$$

From geometrical considerations, the projected contact area for the spherical indenter and the contact point radius (see Fig. 2a) is

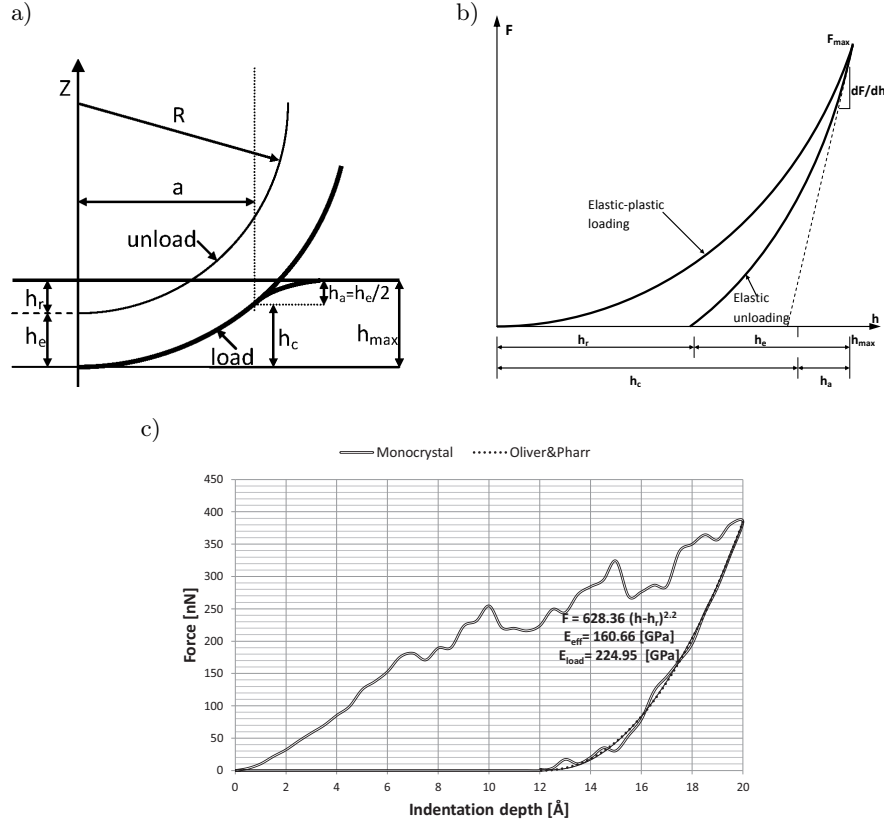


Fig. 2. a) A schematic of the spherical indenter where bold lines denote a line-surface of the indenter at two indentation depths. b) A schematic of the force-depth curve for the indentation model where bold lines denote the loading-unloading curve (for further details see main text and also [7]). c) The calculated force-depth curve for monocrystalline sample.

$$(3.6) \quad A_c = \pi a^2 = \pi(2Rh_c - h_c^2),$$

giving the indentation modulus  $E_{\text{eff}}$  for unloading as

$$(3.7) \quad E_{\text{eff}} = \frac{1}{2} \frac{dF}{dh} \sqrt{\frac{\pi}{A_c}} = \frac{1}{2} S_{\text{max}} \sqrt{\frac{\pi}{A_c}}.$$

For the load path of the indentation curve, if the applied force  $F_h$  at some arbitrary depth  $h$  is known, the contact depth can be readily determined by:

$$(3.8) \quad h_c \approx h - \frac{h_e}{2} = h - \frac{3F_h}{4S_h}.$$

In general, the contact stiffness  $S_h$  in Eq. (3.8) can be different for each indentation step, but following the approach presented in [21], instead of the variable  $S_h$  we use a fixed  $S_{\text{max}}$  appointed in Eq. (3.5). By combining that with relation (3.6) (see

Fig. 2), the contact area during any point of elasto-plastic loading can be obtained. It should be noted that for the purely elastic regime,  $h_c = h/2 = h_e/2$ , whereas for the most part in the plastic regime,  $h \gg h_e/2$  (see Eq. 3.8) and hence  $h_c \approx h$ ; for more details see [18]. Normalisation of the load by the projected contact area gives the mean contact pressure known as the indentation stress, or “Meyer hardness” [7, 23], which can be expressed in the elastic realm of deformation by:

$$(3.9) \quad \frac{F}{A_c} = \frac{4}{3\pi} E_{\text{eff}} \left( \frac{a}{R} \right),$$

where the expression in parentheses on the right-hand side represents the indentation strain. Note that these are not the same as the stresses and strains measured in uniaxial compression tests [18]; and it can be shown that the Meyer hardness is less sensitive to the applied load and a more fundamental measure of indentation hardness than the Brinell hardness [27].

### 3.1. Verification of method of deducing the contact area

To verify correctness of the prescribed above method of calculating the contact area, its values are also measured by analysis of regular “snapshots” of the indentation steps for monocrystalline copper. During indentation, the relative positions of atoms are calculated as well as the symmetric per-atom stress tensor according to [22]. Based on displacements, the Ackland parameter depicted in Fig. 3 and the  $zz$ -component of the per-atom stress tensor, the “real” contact area can be determined [8, 29].

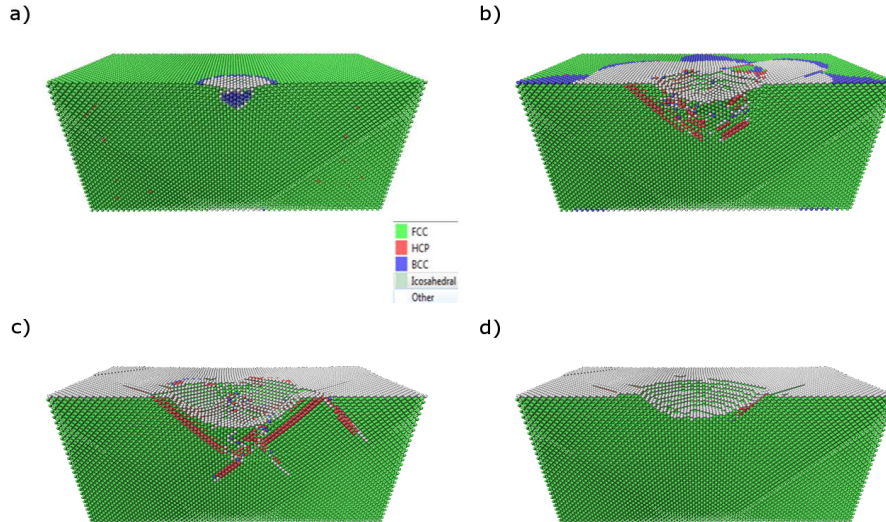


FIG. 3. The same as in Fig. 1 for monocrystalline copper during four states of nanoindentation: a) 4 Å, b) 12 Å, c) 20 Å, d) full unloading.

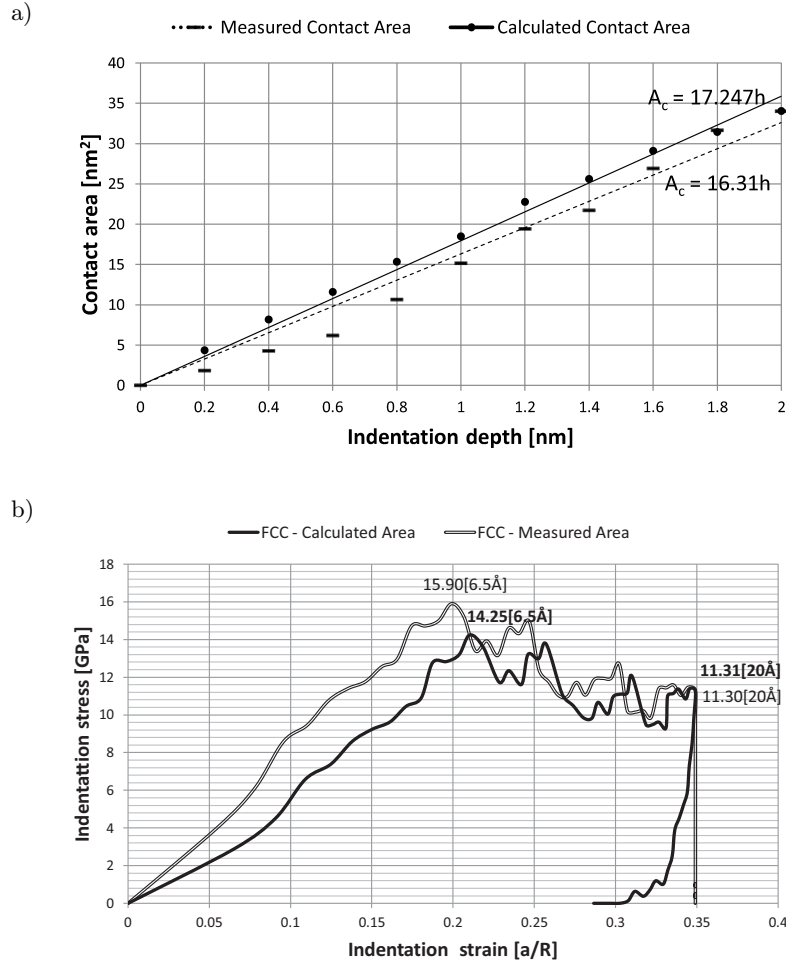


FIG. 4. Measured and calculated quantities for monocystal copper: a) contact area with respect to the indentation depth; b) indentation stress-strain curves.

Comparison of the calculated and measured contact area are given in Fig. 4a. The deviation of one from the other is most pronounced during the mid-stage of loading (cf. elastic-plastic regime) and is recovered toward the end of the process. This leads to an overestimation of the indentation stress-strain relation, see Fig. 4b. In any case, it is given that for all indentation cases the calculated contact area equals the measured one for a maximum load and can be rationally approximated by a linear function of the depth of indentation. This approximation for the contact area is used in this work. Thus, an additional relation may be drawn for the calculated mean contact pressure, and the indentation stress (utilising the linear approximation of contact area) against the indentation strain

next to the classical force-depth curve (Fig. 5). For comparison, the classical hardness during indentation is calculated from the maximum force related to the residual imprint of the indenter [9].

A planar indenter is really an infinitely extended axis-aligned wall, exerting the same force on atoms in the system across the contact area as in Eq. (3.1), but where  $R$  is the position of the plane and  $r - R$  is the distance from the plane [22]. As in the case of spherical indentation described above, the planar indenter is

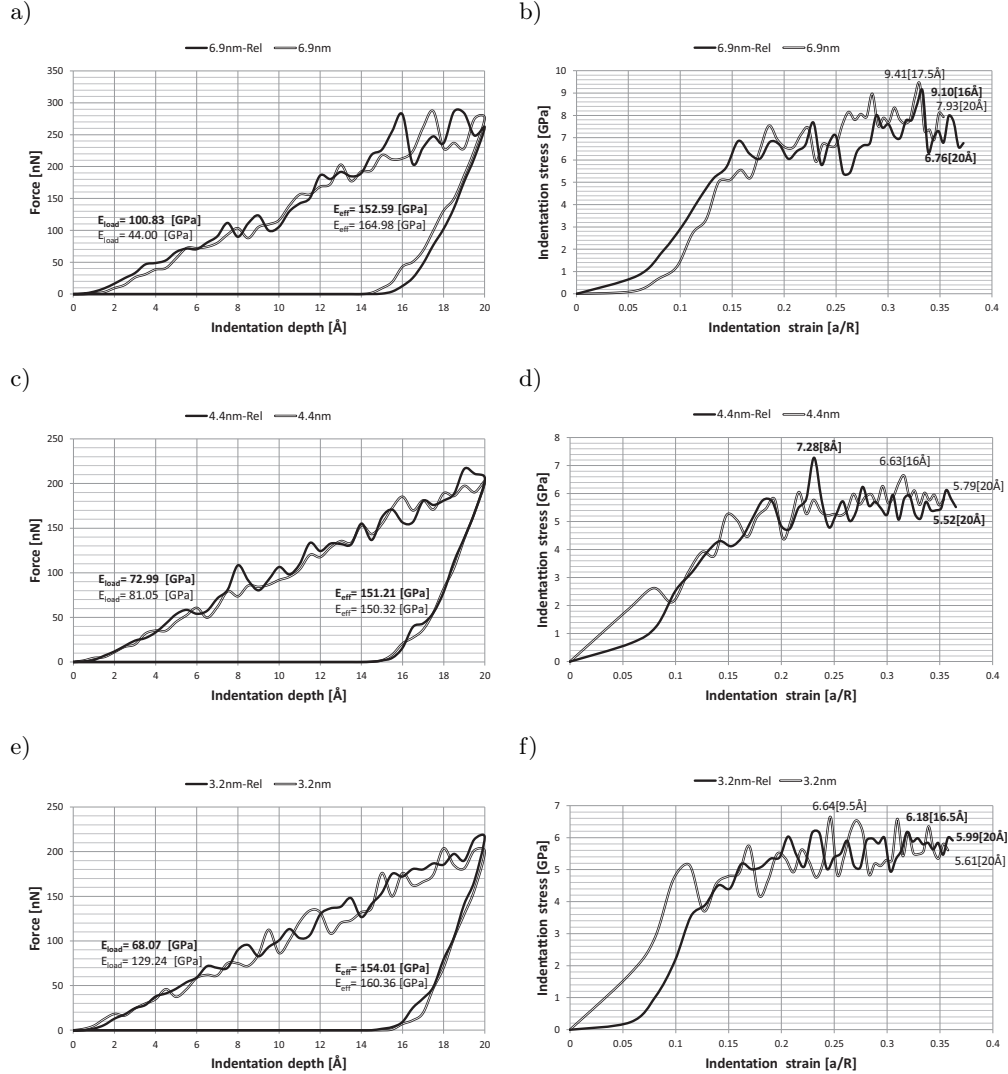


Fig. 5. The force-depth curve, the calculated indentation modulus (left panel) and the indentation stress-indentation strain curve (right panel). From top-to-bottom: copper grains of size: 6.9 nm, 4.4 nm, and 3.2 nm.

moved down in steps  $\Delta h = 0.5 \text{ \AA}$  up to a depth of  $4 \text{ \AA}$  which corresponds to  $\sim 4\%$  of indentation strain, and then withdrawn. The ratio between indentation stress, calculated as indenter force divided by a cross-sectional area of the sample against the indentation strain ( $h/l$ ), is an analog of the indentation modulus  $E_{\text{eff}}$  in Eq. (3.7).

$$(3.10) \quad \frac{F}{A} = E_{\text{eff}} \left( \frac{h}{l} \right),$$

where  $l$  is the thickness of the sample. Owing to the boundary constraints applied here, deformation of the sample resembles a uniaxial strain deformation (zero strain in the plane perpendicular to the indentation direction). In fact, the deformation for a monocrystal strained along crystallographic axis yields the result that  $E_{\text{eff}}$  is equal to the  $C_{11}$  modulus of fcc copper crystal.

#### 4. Results and discussion

The vertical motion of the indenter is divided into several steps and on each step a MS calculation is performed to minimise internal energy until the change between consecutive iterations is less than  $E_{\text{tol}} < 10^{-8}$ , and the  $\ell_2$ -norm of the global force vector is less than  $F_{\text{tol}} < 10^{-8}$ . MD and MS relaxed samples were tested by a spherical indentation and by the comparative method of planar indentation. Simulations carried out in this work, performed sequentially on AMD Athlon™ 600e, 2.2 GHz processor require: (i) The preresolution step using MD consumed approximately  $\sim 12$  hours of user's time; (ii) The preresolution step in MS consumed approximately 2 hours of user's time (a factor of  $\sim 6$  less). Moreover, the MS simulation, using instantaneous relaxation and 80 steps of the nanoindentation process (40/40 for loading/unloading), consumed  $\sim 12$  hours of user's time: *that is around the same time required for a single MD step.*

The influence of the preparation of a computable sample on the obtained result is examined, i.e. indentation curves: force-depth (left panel of Fig. 5) and stress-strain (right panel of Fig. 5); and the material parameters, hardness and elastic modulus (see also Fig. 6). An analysis of the force-depth curves for preresolved and instantaneously relaxed samples show no significant difference between the two mentioned methods. The results and behaviour of monocrystalline copper are very similar to the results from [14, 15]. It is however difficult to find a general correlation between the two methods of sample relaxation on the basis of the indentation stress-strain curve. At the initial stage of nanoindentation where the depth  $d \lesssim 1.0 \text{ \AA}$ , the curves differ somewhat more than in the final stages of loading.

The indentation moduli calculated on the basis of elastic loading part (Eq. 3.2) differs significantly from these calculated from elastic unloading part

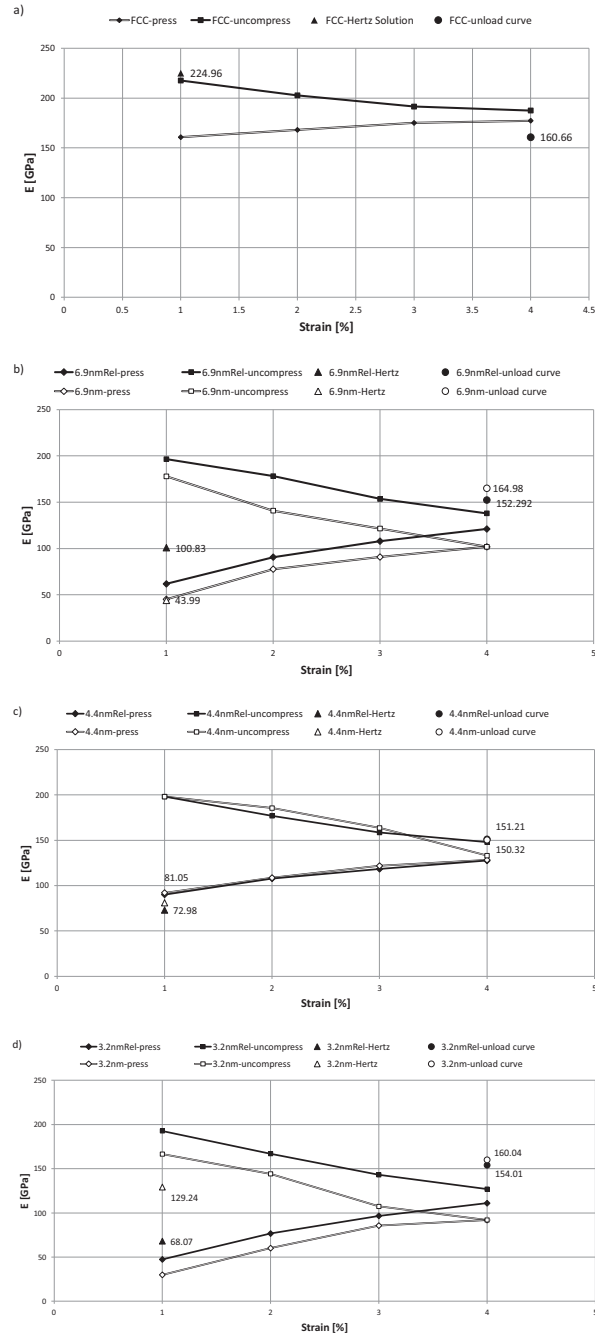


Fig. 6. Calculated effective modulus for planar (loading and unloading curve) and spherical indenter (Hertz solution–1% of indentation strain and unloading curve) for relaxed and instantaneously relaxed samples: a) monocrystal, b) 6.9 nm grain copper, c) 4.4 nm grain copper, d) 3.2 nm grain copper.

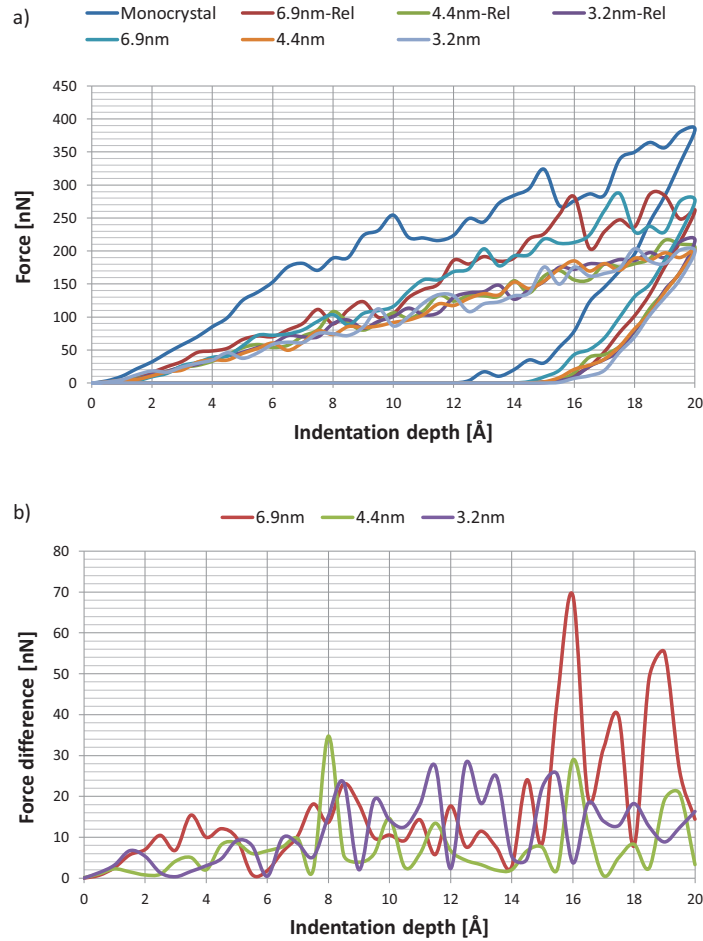


Fig. 7. A collective summary of the main results of the nanoindentation process considered in this work: a) the force-indentation curves for all mono and polycrystalline copper samples; b) summary of the difference of the indentation force between simulations, done with preresolution and instantaneous relaxation (polycrystalline samples only).

(Eq. 3.7) and show a high level of irregularity. The stiffness modulus  $E_{\text{eff}}$  averaged over the first four indentation steps ( $2.0 \text{ \AA}$  corresponds to  $\sim 2\%$  of the sample thickness and indentation strain  $a/R \sim 0.1$ ); these values are comparable to those in [19]. Up to this level, an increase of calculated stiffness modulus is found, which can be treated as an indication of elasticity. After this the material should be considered as being within the elastic-plastic regime.

The results of Fig. 7a qualitatively agree with the indentation study on mono- and polycrystalline copper in [2], and in particular that the indentation forces for monocrystalline material are higher than those found for poly-

crystalline material. This trend was determined here for the range of grain sizes  $\in \{3.2, 4.4, 6.9\}$  nm, in which the force-displacement curve for smaller grain size always lies below that of the same displacement curve for larger grain size (see Fig. 7a). It is known that indentation in the elastic range is strongly affected by surface roughness and initiation of contact, so determination of the indentation modulus in a such way is not always very reliable. A more reliable method is to determine the effective moduli from the elastic unloading curve [7, 21] and hence, very similar results in the range of  $150 \lesssim E_{\text{eff}} \lesssim 164$  GPa were found. This translates to around 10% dispersion for any given sample. The calculated effective modulus  $E_{\text{eff}}$  agrees with experimental observations [25]. The indentation modulus calculated on the basis of planar indentation test tends to rise during loading and fall during unloading. Coincidentally, the indentation modulus  $E_{\text{eff}}$  measured for maximal compression of the sample ( $\sim 4\%$  of the indentation strain) corresponds to the indentation modulus found using a spherical indentation determined from the unloading part of the test (Fig. 6).

The maximum value of the Meyer hardness was found to be 15.9 GPa (Section 3) for monocrystal copper (Fig. 4) which agrees well with a result from [24, 35, 36]; whereas additionally, the classical hardness was found to be 11.31 GPa. For polycrystalline copper it is difficult to find a clear relationship between the prerelaxation type and hardness for both the Meyer and classical hardness (Fig. 5). In general it can be stated that: with decreasing grain size, a decrease in the Meyer and classical hardness is observed. This is a demonstration of the inverse Hall–Petch relation [4, 31], i.e. that from some critical level of grain size ( $\sim 10$  nm) the yield strength decreases with reduction of the grain size.

## 5. Summary

The force-indentation curve that describes the loading and unloading cycle of the nanoindentation process is summarised in Fig. 7a. The fact is that the forms of the results are qualitatively the same, irrespective of the prerelaxation method used is satisfying (cf. Fig. 5). It is also noticeable that a smaller grain size does not result in a stiffer material. An open question arises here: “Whether (and if so – where?) a critical grain size to hardness relation exists for copper?” Fig. 7b gives the modulus of the difference between the force-indentation curves computed for nanoindentation starting from the material relaxed with MD and the material instantaneously relaxed with MS. It is worth emphasising here that the variations in the curves do not give any error indicator, but rather directly illustrate a sensitivity of simulation on the starting point of a nanoindentation process. This indicates that a statistical approach to gathering of information from nanoindentation simulations may be preferable to “one-shot” investigations (as suggested in Section 1). Statistical gathering of information on the nanoin-

dentation process is made computationally amenable by fast relaxation methods, such as the instantaneous relaxation used in this work. It is satisfying therefore that from the results presented here, it seems that the usual time-consuming MD approach to molecular relaxation is justified but not necessary for successful qualitative modelling of the nanoindentation process by empirical potentials.

In summary, it has been shown that:

1. The numerical behaviour of the nanoindentation process following instantaneous relaxation is stable and produces sensible results without resorting to more time-consuming techniques (i.e. preresolution by MD).
2. There is no discernible influence of the chosen method of preparation of a computable sample due to preresolution of structure on the calculated parameters: hardness, elastic modulus, force-depth and indentation stress-strain curves; and c.f. Fig. 5.
3. Monocrystal and polycrystal samples, regardless of grain size, have a similar value of indentation modulus lying in the range  $150 \leq E_{\text{eff}} \leq 164$  GPa; cf. Fig. 6.
4. The inverse Hall–Petch relation, i.e. the Meyer and classical hardness decreases with reduction of the grain size and is significantly lower than the hardness of a monocrystal.
5. The indentation modulus should be determined from the unloading curve, not the loading one such that the appointed modulus shows good agreement with that of planar indentation.

### Acknowledgements

The research was funded, with the financial support of the Project R1501203, by the Polish Ministry of Science and Higher Education.

### References

1. G.J. ACKLAND, A.P. JONES, *Applications of local crystal structure measures in experiment and simulation*, Phys. Rev. B, **73**, 2006.
2. A.V. BOLESTA, V.M. FOMIN, *Molecular dynamics simulation of sphere indentation in a thin copper film*, **12**, 3–4, 117, 2009.
3. F. CLERI, V. ROSATO, *Tight-binding potentials for transition metals and alloys*, Phys. Rev. B, **48**, 1993.
4. H. CONRAD, J. NARAYAN, *On the grain size softening in nanocrystalline materials*, Scripta Materialia, **42**, 11, 2000.
5. P. DŁUŹEWSKI, P. TRACZYKOWSKI, *Numerical simulation of atomic positions in quantum dot by means of molecular statics*, Archives of Mechanics, **55**, 2003.

6. D. FEICHTINGER, P.M. DERLET, H. VAN SWYGENHOVEN, *Atomistic simulations of spherical indentations in nanocrystalline gold*, Phys. Rev. B, **67**, 2003.
7. A.C. FISCHER-CRIPPS, *Nanoindentation*, Springer-Verlag, New York, USA, 2004.
8. Y.-R. JENG, CH.-M. TAN, *Static Atomistic Simulations of Nanoindentation and Determination of Nanohardness*, J. Appl. Mech., **72**, 2005.
9. S. P. JU, C.T. WANG, C.H. CHIEN, J.C. HUANG, S.R. JIAN, *The nanoindentation responses of nickel surfaces with different crystal orientations*, Mol. Simul., **33**, 2007.
10. E. KIMMARI, L. KOMMEL, *Application of the continuous indentation test method for the characterization of mechanical properties of B<sub>4</sub>C/Al composites*, Proc. Estonian Acad. Sci. Eng., **12**, 2006.
11. J. KNAP, M. ORTIZ, *An analysis of the quasicontinuum method*, J. Mech. Phys. Solids, **49**, 2001.
12. A. LATAPIE, D. FARKAS, *Molecular dynamics investigation of the fracture behavior of nanocrystalline  $\alpha$ -Fe*, Phys. Rev. B, **69**, 2004.
13. J. LI, *AtomEye: an efficient atomistic configuration viewer*, Modelling Simul. Mater. Sci. Eng., **11**, 2003.
14. H. LIANG, C.H. WOO, HANCHEN HUANG, A.H.W. NGAN, T.X. YU, *Crystalline Plasticity on Copper (001), (110), and (111) Surfaces during Nanoindentation*, Comp. Model. Eng. Sci., **6**, 2004.
15. H.Y. LIANG, C.H. WOO, HANCHEN HUANG, A.H.W. NGAN, T.X. YU, *Dislocation nucleation in the initial stage during nanoindentation*, Phil. Mag., **83**, 2003.
16. Y.-H. LIN, T.C. CHEN, *A molecular dynamics study of phase transformation in monocrystalline Si under nanoindentation*, Appl. Phys. A, **92**, 571, 2008.
17. M. MAŁDZIARZ, T.D. YOUNG, P. DŁUŻEWSKI, T. WEJRZANOWSKI, K.J. KURZYDŁOWSKI, *Computer modelling of nanoindentation in the limits of a coupled molecular-statics and elastic scheme*, J. Comput. Theor. Nanosci., **7**, 1172, 2010.
18. A.J. MOSESON, *Spherical Nanoindentation: Insights and Improvements, Including Stress-Strain Curves and Effective Zero Point Determination*, M.Sc. Thesis, Drexel University, Philadelphia, USA, 2007.
19. A.K. NAIR, D. FARKAS, R.D. KRITZ, *Molecular dynamics study of size effects and deformation of thin films due to nanoindentation*, CMES, **24**, 3, 239, 2008.
20. A. OKABE, B. BOOTS, K. SUGIHARA, *Spatial Tessellations: Concepts and Applications of Voronoi Diagrams*, John and Wiley & Sons, New York, USA, 1992.
21. W. C. OLIVER AND G. M. PHARR, *Measurement of hardness and elastic modulus by instrumented indentation: Advances in understanding and refinements to methodology*, J. Mater. Res., **19**, 2004.
22. S. J. PLIMPTON, *Fast Parallel Algorithms for Short-Range Molecular Dynamics*, J. Comp. Phys., **117**, 1995, (<http://lammps.sandia.gov>).
23. J.J. ROA, E. JIMENEZ-PIQUE, X.G. CAPDEVILA, M. SEGARRA, *Nanoindentation with spherical tips of single crystals of YBCO textured by the Bridgman technique: Determination of indentation stress-strain curves*, J. of the European Ceramic Society, **30**, 2010.

24. CH. SHANGDA, K.E. FUJIU, *MD simulation of the effect of contact area and tip radius on nanoindentation*, Science in China Ser. G Physics and Astronomy, **47**, 2004.
25. D.J. SHUMAN, A.L.M. COSTA, M.S. ANDRADE, *Calculating the elastic modulus from nanoindentation and microindentation reload curves*, Materials Characterization, **58**, 2007.
26. A. STUKOWSKI, *Visualization and analysis of atomistic simulation data with OVITO – the Open Visualization Tool*, Modelling Simul. Mater. Sci. Eng., **18**, 2010.
27. D. TABOR, *The Hardness of Metals*, Oxford University Press, 2000.
28. E.B. TADMOR, M. ORTIZ, R. PHILIPS, *Quasicontinuum analysis of defects in solids*, Phil. Mag., **A73**, 1996.
29. CH.-M. TAN, Y.-R. JENG, *Computer simulations of nanoindentation on Cu (111) with a void*, Int. J. Sol. Struct., **46**, 2009.
30. T. TSURU, Y. SHIBUTANI, Y. KAJI, *Nanoscale contact plasticity of crystalline metal: Experiment and analytical investigation via atomistic and discrete dislocation models*, Acta Materialia, **58**, 2010.
31. H. VAN SWYGENHOVENA, J.R. WEERTMAN, *Deformation in nanocrystalline metals*, Materials Today, **9**, 2006.
32. O.G. VINOGRADOV, *On reliability of molecular statics simulations of plasticity in crystals*, Computational Materials Science, **50**, 2010.
33. K. YASHIRO, A. FURUTA, Y. TOMITA, *Nanoindentation on crystal/amorphous polyethylene: Molecular dynamics study*, Comp. Mat. Sci., **38**, 136, 2006.
34. S. YIP, *Handbook of Materials Modeling*, Springer Science and Business Media, 2005.
35. G. ZIEGENHAIN, A. HARTMAIER, H.M. URBASSEK, *Pair vs many-body potentials: Influence on elastic and plastic behavior in nanoindentation of fcc metals*, J. Mech. Phys. Solids, **57**, 2009.
36. G. ZIEGENHAIN, H.M. URBASSEK, A. HARTMAIER, *Influence of crystal anisotropy on elastic deformation and onset of plasticity in nanoindentation: A simulational study*, J. Appl. Phys., **107**, 2010.

*Received December 29, 2010; revised version July 2, 2011.*

---